PHYSICAL REVIEW A **93**, 053618 (2016)

Work fluctuations in bosonic Josephson junctions

R. G. Lena,[1] G. M. Palma,[2] and G. De Chiara[3]
[1]*Dipartimento di Fisica e Chimica, Università di Palermo, via Archirafi 36, 90123 Palermo, Italy*
[2]*NEST, Istituto Nanoscienze-CNR and Dipartimento di Fisica e Chimica, Università degli Studi di Palermo, via Archirafi 36, I-90123 Palermo, Italy*
[3]*Centre for Theoretical Atomic, Molecular and Optical Physics, School of Mathematics and Physics, Queen's University, Belfast BT7 1NN, United Kingdom*
(Received 23 March 2016; published 23 May 2016)

We calculate the first two moments and full probability distribution of the work performed on a system of bosonic particles in a two-mode Bose-Hubbard Hamiltonian when the self-interaction term is varied instantaneously or with a finite-time ramp. In the instantaneous case, we show how the irreversible work scales differently depending on whether the system is driven to the Josephson or Fock regime of the bosonic Josephson junction. In the finite-time case, we use optimal control techniques to substantially decrease the irreversible work to negligible values. Our analysis can be implemented in present-day experiments with ultracold atoms and we show how to relate the work statistics to that of the population imbalance of the two modes.

DOI: 10.1103/PhysRevA.93.053618

I. INTRODUCTION

Thermodynamics has lasted through all the scientific revolutions that have occurred in the last centuries. In the early days, thermodynamics was applied to macroscopic systems with a number of particles of the order or larger than the Avogadro number. This implies that when repeating a thermodynamic process under the same conditions, the observed values of thermodynamic quantities, such as work, entropy, and heat, would always be the same. Recently, motivated by experiments in mesoscopic systems in solid-state physics, molecular biology, and in optical and atomic physics, attention has been turned to the fluctuations of thermodynamic quantities satisfying fundamental theorems [1,2]. Such fluctuations can have a twofold origin: they can be merely due to the smallness of mesoscopic systems giving rise to classical statistical fluctuations; or, they can be intrinsically quantum fluctuations.

In the context of work in quantum mechanics, it has been shown that work cannot be identified with a single observable but rather to a generalized measurement [3–8]. Quantum fluctuations of work, in contrast to classical thermal fluctuations, survive when the temperature is lowered close to absolute zero. Their origins can be traced to the noncommutativity of operators in quantum mechanics: they emerge when driving a system with a sequence of Hamiltonians that do not commute with each other [9]. Such observation leaves an open question: How can one access the quantum fluctuations of work for a quantum mesoscopic system?

The aim of this paper is to answer positively to this question by studying the fluctuations of work generated by or made on a system of ultracold atoms in a double-well potential. Recent technological and experimental progress in the field of cold atomic gases has triggered enormous research activity towards the realization of quantum simulators of condensed-matter physics models, quantum metrology, and quantum information processors [10–12]. Far less attention has been devoted to applications of out-of-equilibrium thermodynamics in ultracold atoms [7] with the exception of the issue of thermalization in closed quantum systems [13,14].

Here, we consider a zero-temperature bosonic gas subject to a double-well potential. In the so-called two-mode approximation, the system can be regarded as a bosonic Josephson junction [15,16] and its physics has been extensively studied both theoretically [17–21] and experimentally [22–27]. We calculate the work fluctuations in such setup after changing the interparticle interaction strength by means of a Feshbach resonance. Similar effects could be obtained by changing the potential, raising or lowering the barrier separating the two wells. For slow adiabatic changes of the interaction, the work needed to drive the system is approximately given by the free-energy difference ΔF of the initial and final equilibrium states. However, for fast driving the average work is always larger than ΔF and their difference gives the irreversible work. We analyze the dependence of the irreversible work on the initial and final values of the self-interaction constant spanning the Rabi, Josephson, and Fock regime of the double-well system.

Furthermore, with the aim of reducing the irreversible work production, we employ optimal control methods to find a tailored time-dependence of the self-interaction [28]. We find that the irreversible work can be effectively reduced to a negligible value even if driving the system at a finite speed, challenging the minimal work principle [29]. We test the robustness of our protocol to imperfections in the values of the self-interaction.

Our results can be tested in present-day experiments with ultracold atoms in double-well potentials [22–27] or realizing instances of the Lipkin-Meshkov-Glick (LMG) [30,31] as, for instance Bose-Einstein condensates in optical cavities [32]. In Sec. VI, we discuss a scheme to estimate work fluctuations in such systems.

II. MODEL

The system considered is a zero-temperature Bose-Einstein condensate in a double-well potential. For our study we use the two-mode Bose-Hubbard Hamiltonian

$$\hat{H} = \frac{U}{2}[\hat{n}_L(\hat{n}_L - 1) + \hat{n}_R(\hat{n}_R - 1)] - J(\hat{a}_L\hat{a}_R^\dagger + \hat{a}_R\hat{a}_L^\dagger), \tag{1}$$

where J and U are respectively the tunneling and the self-interaction energies and the number of particles N is assumed

to be constant. The operators $\hat{a}_L$ and $\hat{a}_R$ are the particle annihilation operators in the left and right well, respectively, and $\hat{n}_L$ and $\hat{n}_R$ are the corresponding number operators.

We analyze the system by using both a numerical and an analytical approach in order to find the eigenstates of the Hamiltonian. The analytical results are obtained by mapping the double well to a quantum harmonic oscillator (QHO). In order to do that, we introduce the Schwinger operators

$$\hat{J}_x = \frac{1}{2}(\hat{a}_R^\dagger \hat{a}_R - \hat{a}_L^\dagger \hat{a}_L), \tag{2}$$

$$\hat{J}_y = \frac{i}{2}(\hat{a}_R^\dagger \hat{a}_L - \hat{a}_L^\dagger \hat{a}_R), \tag{3}$$

$$\hat{J}_z = \frac{1}{2}(\hat{a}_L^\dagger \hat{a}_R + \hat{a}_R^\dagger \hat{a}_L), \tag{4}$$

fulfilling the standard angular momentum commutation relations: $[\hat{J}_x, \hat{J}_y] = i\hbar \hat{J}_z$. These operators allow us to describe the system with the angular momentum formalism obtaining the Hamiltonian in the form

$$\hat{H} = -\frac{U}{2}N + U\left(\frac{N}{2}\right)^2 + U\hat{J}_x^2 - 2J\hat{J}_z. \tag{5}$$

We now map Hamiltonian (5) into that of a QHO employing the Holstein-Primakoff approximation, valid in the Josephson and Rabi regimes [23]. We remind that the system is in the Rabi and the Josephson regimes, respectively, when the conditions $\frac{UN}{J} \ll 1$ and $1 \ll \frac{UN}{J} \ll N^2$ are fulfilled, whereas for $\frac{UN}{J} \gg N^2$ the system is in the Fock regime. The operator $\hat{J}_x$, proportional to the population imbalance, is related to the position operator of the QHO by the equation $\hat{J}_x = \sqrt{N/2}\,\hat{x}$, whereas for the momentum $\hat{p}$ of the QHO it holds the relation $\hat{J}_y = -\sqrt{N/2}\,\hat{p}$. Hence, the double-well system can be mapped to the QHO Hamiltonian

$$\hat{H} = E' + \frac{1}{2}m\omega_p^2\hat{x}^2 + \frac{1}{2m}\hat{p}^2 \tag{6}$$

having an effective mass $m = (2J)^{-1}$ and the plasma frequency $\omega_p = 2J\sqrt{\frac{UN}{2J} + 1}$, where we defined $E' = -U\frac{N}{2} + U\frac{N^2}{4} - J - JN$. While the mapping to Hamiltonian (5) is exact, the mapping to the QHO is only approximate and valid as long as $\langle \hat{a}^\dagger \hat{a} \rangle \ll N$ where $\hat{a} = (\hat{x} + i\,\hat{p})/\sqrt{2}$.

In the following we will need the ground-state expectation values

$$\langle \hat{x}^2 \rangle = \frac{J}{\omega_p} \tag{7}$$

$$\langle \hat{p}^2 \rangle = \frac{\omega_p}{4J} \tag{8}$$

and using the Gaussian properties of the ground state, we obtain

$$\langle \hat{x}^4 \rangle = 3\,\langle \hat{x}^2 \rangle\,. \tag{9}$$

and similarly for other high-order moments.

Within this framework, knowing the eigenstates of the QHO, we are able to compare both numerical and analytical results of the statistics of work, which we now define. Suppose that we prepare a quantum system in the ground state $|\psi_0\rangle$ of an initial Hamiltonian $\hat{H}_i$ with energy E_0. The Hamiltonian is then changed in time, not necessarily in an adiabatic fashion, reaching at time τ the Hamiltonian $\hat{H}_f$ with eigenvalues and eigenstates: $\{\tilde{E}_q, |\tilde{\psi}_q\rangle\}$. The change in the Hamiltonian induces an evolution operator that maps the initial state into $|\psi(\tau)\rangle$. Then, the probability density function of the work done on the system is

$$P(W) = \sum_q |\,\langle \tilde{\psi}_q | \psi(\tau) \rangle\,|^2 \delta(W - \tilde{E}_q + E_0). \tag{10}$$

A similar distribution can be analogously defined for an arbitrary initial state and for nonunitary evolutions.

The average work done for the quench in a finite time, is then obtained as the first moment of $P(W)$:

$$\langle W \rangle = \langle \psi(\tau) | \hat{H}_f | \psi(\tau) \rangle - \langle \psi_0 | \hat{H}_i | \psi_0 \rangle\,. \tag{11}$$

The variance of the work, defined as

$$\Delta W^2 = \langle W^2 \rangle - \langle W \rangle^2\,, \tag{12}$$

with $\langle W^2 \rangle = \langle \psi(\tau) | (\hat{H}_f - E_0)^2 | \psi(\tau) \rangle$, is useful because it gives information about the fluctuations of the work.

Thanks to the Jarzynski relation, it holds the relation $\langle W \rangle \geqslant \Delta F$, where $\Delta F = \tilde{E}_0 - E_0$ is the final-initial ground-state energy difference. Since the equality holds in case of an adiabatic process, in the following we study the irreversible work $W_{\rm irr} = \langle W \rangle - \Delta F$, which measures the amount of wasted work during the transformation.

III. INSTANTANEOUS QUENCH

We start our analysis with an instantaneous quench in which we vary either the self-interaction energy U or the tunneling J. Under this assumption, $|\psi(\tau)\rangle = |\psi_0\rangle$ and the expectation value of (11) is reduced to the evaluation on the ground state of the initial Hamiltonian, hence

$$\langle W \rangle = \langle \psi_0 | (\hat{H}_f - \hat{H}_i) | \psi_0 \rangle = \langle \psi_0 | \hat{H}_f | \psi_0 \rangle - E_0. \tag{13}$$

We evaluate the work done on the system going through all the regimes by keeping fixed U_i and changing U_f and vice versa. By using the mapping to the QHO as shown in Eq. (6) and the results in Eqs. (7)–(9), we find the following analytical results for the average work done on the system, its variance and the irreversible work

$$\langle W \rangle = \Delta U \frac{N}{2}\left[\left(\frac{N}{2} - 1\right) + \frac{J}{\omega_i}\right] \tag{14}$$

$$\Delta W^2 = \frac{J^2}{\omega_i^2}\frac{N^2}{2}\Delta U^2 \tag{15}$$

$$W_i rr = \frac{N}{2}\frac{J}{\omega_i}\Delta U - \frac{\omega_f - \omega_i}{2}. \tag{16}$$

where $\Delta U = U_f - U_i$ and ω_i,ω_f are the initial and final plasma frequencies.

It is important to notice that the average work can be written as

$$\langle W \rangle = W_{\rm class} + W_{\rm quant}, \tag{17}$$

where we want to stress the fact that the average work has a classical constant part $W_{\rm class} = \Delta U \frac{N}{2}(\frac{N}{2} - 1)$ and a quantum

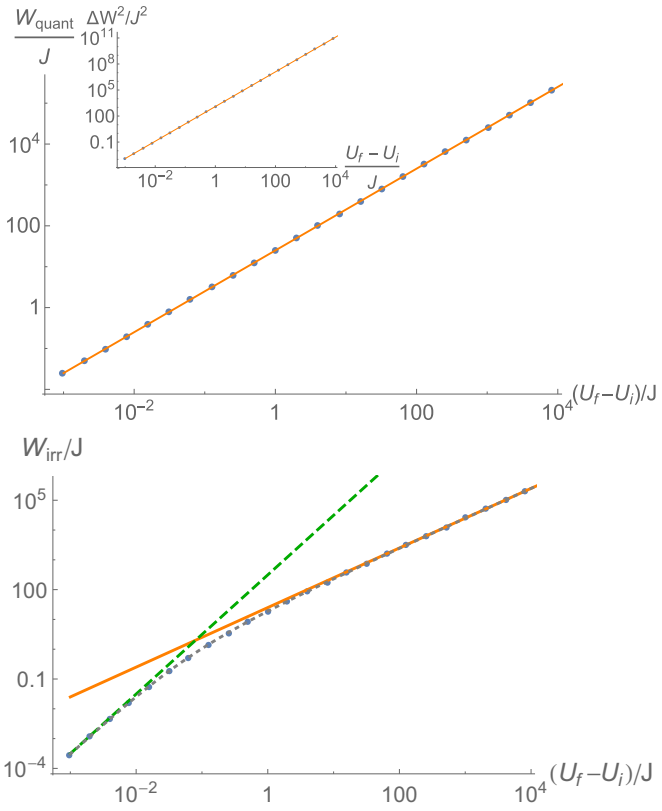

FIG. 1. Numerical (blue dots) and analytical (solid line) log-log plots of the quantum part of the average work (top, main), its variance (inset) and the irreversible work (bottom) against $(U_f - U_i)/J$, obtained by changing U instantaneously from $U_i = 0$, where the system is in the Rabi regime, to different values of U_f in the range $10^{-3}J$–$10^4 J$, including all the regimes for $N = 100$. In the bottom panel, the dotted line fitting the numerical points corresponds to the QHO analytical prediction, the green (dashed) and the orange (solid) lines correspond to the limits $(U_f - U_i)/J$ much smaller and much larger than 1, respectively [see Eqs. (22) and (25)].

part affected by the ground-state quantum fluctuations, related to the average square of the population imbalance

$$W_{\text{quant}} = \Delta U \frac{N}{2} \langle \hat{x}^2 \rangle = \Delta U \langle \hat{n}^2 \rangle , \tag{18}$$

where $\hat{n} = \hat{n}_L - \hat{n}_R$ is the population imbalance.

In Fig. 1 we show the results of the quantum part of the average work, the variance and the irreversible work obtained by varying U, going from a fixed initial value U_i where the system is in the Rabi regime, to different final values U_f belonging to the three regimes.

As expected from the analytical expressions (14)–(16), for the values used in Fig. 1, i.e., $U_i = 0$ implying $\omega_i = 2J$, we obtain $W_{\text{quant}} \approx \frac{N}{4} U_f$ and $\Delta W^2 \approx \frac{N^2}{8} U_f^2$. For the irreversible work the gray dotted line fitting the numerical points is given by the simplified form

$$W_{\text{irr}} = \frac{NU_f}{4} + J - J\sqrt{\frac{U_f N}{2J} + 1} \tag{19}$$

obtained from Eq. (16) with $U_i = 0$.

For this quantity we analyzed two limiting cases: $\frac{U_f N}{2J} \ll 1$ and $\frac{U_f N}{2J} \gg 1$. In the first scenario, by expanding the square-root term up to the second order, i.e., $\sqrt{\frac{U_f N}{2J} + 1} \simeq 1 + \frac{U_f N}{4J} - \frac{U_f^2 N^2}{32J^2}$, we get $W_{\text{irr}} \simeq \frac{N^2}{32J} U_f^2$, represented in Fig. 1 by the green line. On the other hand, when U_f increases and $\frac{U_f N}{2J} \gg 1$, the dominant term is the linear one, and we get $W_{\text{irr}} \simeq \frac{N}{4} U_f$ (orange line).

Analogously, in Fig. 2 we study the case in which we keep fixed the final parameter U_f and vary the initial one U_i going through every of the three regimes of the bosonic Josephson junction. Analogously to the previous case, for the average work, we consider only its quantum component (18).

As expected, the analytical results (green dotted lines) given by Eqs. (18), (15), (16) fit the numerical ones (blue dots) for $U_i < 10^3 J$, because for larger values of U_i, with the parameters used here, the system is in the Fock regime. This limitation of the analytical approach is due to the fact that in this regime the Holstein-Primakoff approximation does not work anymore and the eigenstates of the initial Hamiltonian can not be described as the ones of the QHO. In order to show the results on a log-log graphic, we considered the absolute values of the analyzed quantities, since for $U_i > U_f$, i.e., at the right of the gray dotted line in the graphics, the average work has a negative value, corresponding to work extraction. Furthermore, as done for the previous case in which we change U_f, we analyze the limiting cases for $\frac{U_i N}{2J} \gg 1$ and $\frac{U_i N}{2J} \ll 1$.

For $\frac{U_i N}{2J} \ll 1$ we obtain

$$W_{\text{quant}} \simeq \Delta U \frac{NJ}{4J + U_i N} \tag{20}$$

$$\Delta W^2 \simeq \left(U_f^2 - 2U_f U_i\right) \frac{N^2}{8} \frac{2}{NU_i/(2J) + 1} \tag{21}$$

$$W_{\text{irr}} \simeq \Delta U \frac{N}{4} \frac{1}{1 + U_i N/4J} - \left[\omega_f - 2J\left(1 + \frac{U_i N}{4J} - \frac{U_i^2 N^2}{32J^2}\right)\right] \Big/ 2, \tag{22}$$

where once again we use the expansion

$$\sqrt{\frac{U_i N}{2J} + 1} \simeq 1 + \frac{U_i N}{4J} - \frac{U_i^2 N^2}{32J^2}$$

in series up to the second order, and in (21) we considered $U_i \ll U_f$. These behaviors are shown by the blue lines in Fig. 2.

On the other hand, in the limit for $\frac{U_i N}{2J} \gg 1$, by using the approximation $\sqrt{\frac{U_i N}{2J} + 1} \simeq \sqrt{\frac{U_i N}{2J}}$, we obtained the following analytical results for the examined quantities:

$$W_{\text{quant}} \simeq \frac{\Delta U}{4} \frac{2JN}{U_i} \tag{23}$$

$$\Delta W^2 \simeq -\frac{U_f NJ}{4} - \Delta U \frac{NJ}{4} \tag{24}$$

$$W_{\text{irr}} \simeq \frac{\Delta U}{4} \sqrt{\frac{2JN}{U_i}} - \sqrt{\frac{NJ}{2}} (\sqrt{U_f} - \sqrt{U_i}), \tag{25}$$

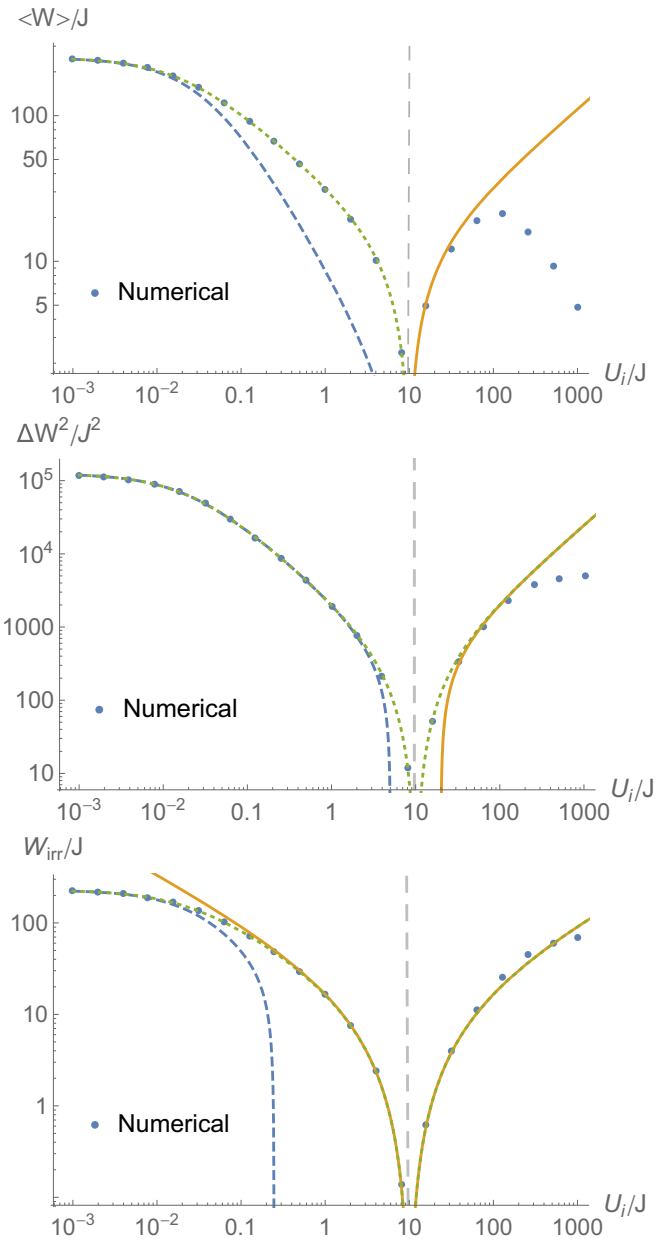

FIG. 2. Analytical (green dotted lines) and numerical (blue dots) log-log plots of the quantum part of the average work (top), its variance (middle) and the irreversible work (bottom) vs U_i, obtained by changing U instantaneously from different values of U_i in the range $10^{-3}J$–$10^{3}J$, including all the regimes, to a value $U_f = 10J$, where the system is in the Josephson regime. We plot the absolute value of the work since it is negative for $U_i \geqslant U_f$. We set $N = 100$. The blue (dashed) and orange (solid) lines represent respectively the analytical formulas obtained for the limiting cases of $\frac{U_i N}{2J} \ll 1$ and $\frac{U_i N}{2J} \gg 1$.

where in (25) we used the approximation $\frac{U_f N}{2J} \gg 1$, since the final state of the system is in the Josephson regime.

So far we have limited our analysis to the first two moments of work and the irreversible work. The full distribution of work can calculated in a similar way. As shown in Eq. (18), the quantum part of the work is proportional to the square of the population imbalance. Since this quantity is approximately

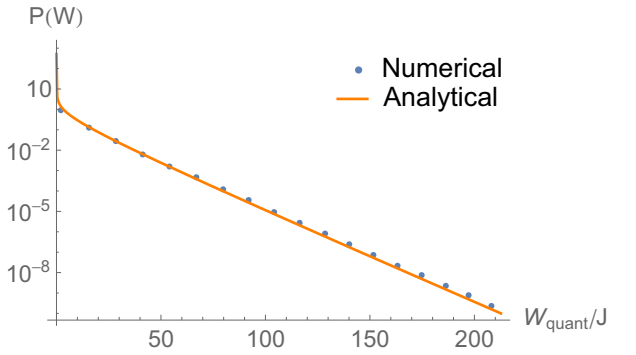

FIG. 3. Semilog plot of the probability distribution of the work calculated analytically by using (26) and numerically, for a sudden quench from $U_i = 0$ to $U_f = 0.1J$ and $N = 100$.

Gaussian in the Rabi and Josephson regime, we expect W_{quant} to be distributed according to an exponential function:

$$P(W_{\text{quant}}) = \sqrt{\frac{N}{\pi \sigma W_{\text{quant}}}} \exp[-W/\sigma] \tag{26}$$

where $\sigma = J\Delta U N/\omega_i$. The relation (26) works quite well in the Josephson regime as shown in Fig. 3. As it can be noticed from this plot, for higher values of the work, the analytical and numerical results present a progressive slight shift. This is probably due to the fact that in the Holstein-Primakoff approximation we are neglecting higher-order terms, hence the spacing between the energy levels in the Bose-Hubbard model may not be exactly the same as in the QHO.

IV. FINITE-TIME TRANSFORMATIONS

We now turn to a transformation in which we vary the work parameter U in a finite time τ. As we saw in the previous sections, the properties of the bosonic Josephson junction are well captured by the QHO away from the Fock regime. We thus expect that even for the dynamics such mapping still holds. In our analysis, we compare the numerical results obtained for the work fluctuations by using the Bose-Hubbard model with the semianalytical results obtained from the approach of Ford *et al.* [33] for the evolution of the ground state in a QHO with a time-dependent frequency (see Appendix A for the detailed calculations). Previous works have investigated the work distribution of a QHO, for the case of a linear ramp for the squared frequency [34], i.e., $\omega^2(t) = \omega_0^2 - (\omega_0^2 - \omega_1^2)t/\tau$, and for a generic ramp [33].

We start our analysis with a linear ramp for $U(t)$:

$$U_{\text{lin}}(t) = U_i + (U_f - U_i)\frac{t}{\tau}. \tag{27}$$

The results for the variance of work and irreversible work are shown in Fig. 4. In order to compare the numerical results with the time evolution of the QHO, we notice that since the plasma frequency squared is a linear function of $U(t)$, for the ramp in Eq. (27), we are considering the same case of Ref. [34]. The results show that both irreversible work and variance of work decay with the ramp duration τ. This is analogous to the analysis in Ref. [34] with the adiabaticity parameter Q. Moreover, we observe oscillations in both quantities as

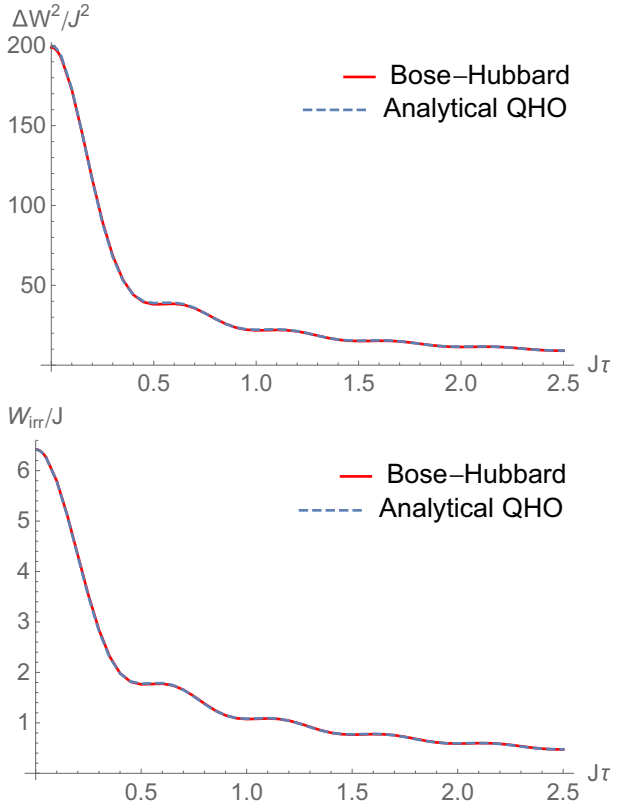

FIG. 4. Analytical (dashed) and numerical (solid) plots of variance of the work (top) and the irreversible work (bottom) vs τ, obtained by changing U from $U_i = 0$ to $U_f = 0.2J$ with $N = 200$.

a function of τ. These can be associated with parametric time oscillations of the variance of the population imbalance around the variance of the instantaneous ground state. Thus, the irreversible work is directly related to squeezing and antisqueezing of the population imbalance in time. Such conjecture is confirmed in Appendix A.

Furthermore, having a semianalytical form of the transition probability $p^{\tau}_{q,0}$ (A10), we obtain both numerical and analytical results for the probability distribution of the work, defined as

$$P(W) = \sum_q \left|p^{\tau}_{q,0}\right|^2 \delta(W - q\omega_i). \tag{28}$$

Even in this case, we obtain a shift between numerical and analytical results similar to the one obtained for a sudden quench, shown in Fig. 3.

V. OPTIMAL CONTROL

It is natural to expect that for a given duration τ, the irreversible work should depend on the actual time dependence of the self-interaction $U(t)$. The aim of this section is to find the best ramp $U(t)$ that minimizes $W_{\rm irr}$ for fixed τ. Previous attempts to reduce irreversible work in quantum harmonic oscillators [35,36] and systems within the linear response regime [37] have been reported. Our goal is a standard optimal control problem [38], which we approach considering two types of chopped basis: the first a linear ramp plus a truncated Fourier expansion, similar to Ref. [28], and a polynomial.

For these functions we impose the boundary conditions $U(0) = U_i$ and $U(\tau) = U_f$ and we enforce the plasma frequency $\omega(t) = 2J\sqrt{\frac{U(t)N}{2J} + 1}$ to be real for every t. We optimized the free parameters of every kind of ramp and compared the results of the irreversible work with the case of the linear ramp $U_{\rm lin}(t)$, Eq. (27).

In a first attempt, we use one ramp from each class with four parameters of which, given the boundary conditions, two are free. The first one is a linear ramp with two sinusoidal terms, having the form

$$U_{\rm LCS}(t) = A_0 + A_1 \cos\left(\frac{\pi t}{\tau}\right) + B_1 \sin\left(\frac{\pi t}{\tau}\right) + C_1 \frac{t}{\tau} \tag{29}$$

with $A_0 = U_i - A_1$ and $C_1 = U_f - U_i + 2A_1$ in which we optimize the free parameters A_1 and B_1. The frequency of the oscillating terms is chosen to have at least one oscillation during the ramp. The second kind of ramp analyzed is a cubic polynomial:

$$U_c(t) = A_0 + A_1 \frac{t}{\tau} + A_2 \left(\frac{t}{\tau}\right)^2 + A_3 \left(\frac{t}{\tau}\right)^3, \tag{30}$$

where the free parameters A_2 and A_3 are optimized. For this case the boundary conditions impose $A_0 = U_i$ and $A_1 = U_f - U_i - A_2 - A_3$.

For comparison we consider also other ramps with four free parameters. In the first one we add two frequencies to the ramp $U_{\rm LCS}(t)$, hence we consider A_1, B_1, A_2, and B_2 as free parameters in

$$U_{\rm 2LCS}(t) = A_0 + A_1 \cos\left(\frac{\pi t}{\tau}\right) + B_1 \sin\left(\frac{\pi t}{\tau}\right) + A_2 \cos\left(\frac{2\pi t}{\tau}\right) + B_2 \sin\left(\frac{2\pi t}{\tau}\right) + C_1 \frac{t}{\tau}. \tag{31}$$

The last ramp we consider is a quintic polynomial:

$$U_q(t) = A_0 + A_1 \frac{t}{\tau} + A_2 \left(\frac{t}{\tau}\right)^2 + A_3 \left(\frac{t}{\tau}\right)^3 + A_4 \left(\frac{t}{\tau}\right)^4 + A_5 \left(\frac{t}{\tau}\right)^5. \tag{32}$$

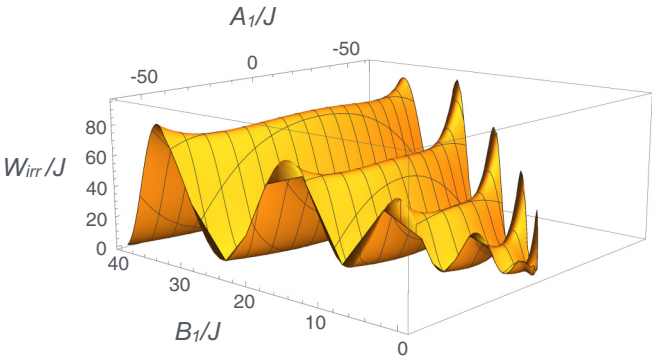

FIG. 5. Irreversible work vs the parameters A_1 and B_2 calculated for the ansatz $U_{\rm LCS}(t)$ (Linear + Cos + Sin ramp) for the values $U_i = 0.2J$, $U_f = 0.8J$, and $\tau = 0.1/J$.

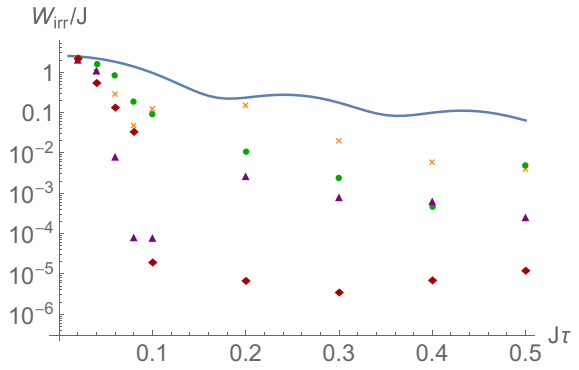

FIG. 6. Semilog plot of the irreversible work vs τ evaluated with the optimal parameters of every ansatz, for values $U_i = 0.2J$ and $U_f = 0.8J$. The blue line corresponds to the linear ramp, the orange crosses to the linear + Sin + Cos ramp, the triangles to the ramp $U_{2\mathrm{LCS}}(t)$, the green points and the diamonds respectively to the cubic and quintic ones.

In each of these cases, the condition of reality imposed on $\omega(t)$ gives a restriction on the possible values of one of the free parameters, depending on the values of the other ones. The choice of the parameters range analyzed is done on the basis of both efficiency and stability, by observing the dependence of the irreversible work on the free parameters which, for the ansatz having two free parameters, can be represented graphically as in Fig. 5. The plot of the irreversible work versus the free parameters for the ramp $U_{\mathrm{LSC}}(t)$ in Fig. 5 shows oscillations of the irreversible work, whose amplitudes increase for larger values of the parameter B_1. Nevertheless, this kind of considerations derived from a graphical representation is hard to extend to the case of more than two free parameters, but we expect a similar potential landscape [39].

The optimized results of the irreversible work obtained for every ramp as a function of the ramp duration τ are compared in Fig. 6 and reported in Table I for convenience. With each of these ramps we obtain a substantial decrease in the dissipated work with respect to the linear ramp for every τ. The most efficient optimizations are obtained with the four-parameters ramps $U_{2\mathrm{LCS}}(t)$ and $U_q(t)$, for which the irreversible work reaches a value smaller than $10^{-4}J$ after a time $\tau = 0.1/J$. For the other ramps the value of the dissipated work is always larger and approaches zero for much higher values of τ. In particular, for smaller values of the duration of the quench, i.e., $0 < J\tau < 0.08$, the ramp U_{LCS} is more efficient than the cubic, but for $0.08 < J\tau < 0.3$, the best optimization is granted by the cubic and the quintic, which reach a zero value of the dissipated work respectively from $\tau = 0.08/J$ and $\tau = 0.1/J$.

On the basis of these results regarding the efficiency of the optimization process, we analyzed the stability of the optimal parameters obtained for every ramp. In order to do that, for every ansatz, we associate a relative percentage error to each parameter, we evaluate the work done on the system for random variations of the parameters inside the range given by the errors, and we consider the average and standard deviation of the irreversible work.

For the case examined above, i.e., $U_i = 0.2J$ and $U_f = 0.8J$, we obtain the maximum stability for the ansatz U_{LCS}, where variations up to the 20% of the optimal parameters give variations on the irreversible work between the 0.2% and the 8%, except for the cases of $\tau = 0.08/J$ and $\tau = 0.1/J$ for which the variations are higher, respectively, of the 13.6% and the 11.4%. The results of this tolerance analysis are shown in Fig. 7. For the cubic ramp, in order to obtain the same kind of results gained for the ramp U_{LCS}, we consider fluctuations of the parameters up to the 5% of their value, obtaining variations in the irreversible work between the 0.5% and the 14%, with higher peaks of the 61.5% and the 40% respectively for $\tau = 0.1J$ and $\tau = 0.3J$. The enhancement in the stability obtained with the ansatz U_{LCS} is due to the fact that, as shown in Fig. 5, variations of A_1 tend to leave the irreversible work in a minimum, hence the major contribution to changes in the value of the work is given by B_1. On the other hand, for the cubic ramp, the minima of the oscillations cross different values of both A_2 and A_3, hence both the oscillations contribute to the variations of the irreversible work. Although the ansatz $U_{2\mathrm{LCS}}$ gives the best efficiency, for the values of U analyzed, it is the most unstable. It would probably be possible to minimize the work analyzing a different range of parameters, reducing the efficiency of the optimization in order to enhance its stability, but the lack of a graphical representation for the case of four free parameters analysis makes it harder to find a stable range.

TABLE I. Values of the exact optimal parameters and the irreversible work obtained with these for each ramp, for different values of τ, considering a quench from $U_i = 0.2J$ to $U_f = 0.8J$. All quantities are in units of J.

	U_{LCS}			$U_{2\mathrm{LCS}}$					U_c			U_q				
τ	A_1	B_1	W_{irr}	A_1	B_1	A_2	B_2	W_{irr}	A_2	A_3	W_{irr}	A_2	A_3	A_4	A_5	W_{irr}
0.02	3.8	0.2	2.04	3.6	0.4	0.2	0.0	2.01	−8.0	5.4	2.29	−15.8	0.6	16.2	−7.4	2.13
0.04	3.2	0.0	9.47×10^{-1}	21.0	16.0	−6.4	−11.0	1.09	−8.0	5.4	1.63	25.0	−14.0	−21.4	−26.0	5.36×10^{-1}
0.06	3.2	0.0	2.68×10^{-1}	18.0	15.0	3.0	−7.8	7.93×10^{-3}	−8.0	5.6	8.28×10^{-1}	19.6	19.0	−20.2	−26.0	1.31×10^{-1}
0.08	2.2	−0.2	4.45×10^{-2}	1.6	10.4	4.2	−1.4	7.96×10^{-5}	−8.0	5.6	1.90×10^{-1}	2.6	21.0	−2.2	−26.0	3.29×10^{-2}
0.10	1.4	−0.2	1.15×10^{-1}	−15.0	19.8	3.6	−3.8	7.73×10^{-5}	−7.6	5.4	1.84×10^{-3}	4.8	−14.2	8.2	1.2	1.90×10^{-5}
0.20	0.2	−0.2	1.41×10^{-1}	0.2	0.0	−0.6	0.8	2.62×10^{-3}	−0.4	0.6	1.09×10^{-2}	6.8	21.2	−16.8	−17.0	6.67×10^{-6}
0.30	0.0	−0.2	1.86×10^{-2}	3.8	3.2	0.0	−2.6	7.86×10^{-4}	0.0	0.6	2.36×10^{-3}	17.8	−14.0	13.8	−20.4	3.44×10^{-6}
0.40	0.2	−0.2	5.49×10^{-3}	−2.8	−0.4	−3.6	2.4	6.23×10^{-4}	−0.8	1.2	4.59×10^{-4}	10.8	−6.6	2.8	−7.8	6.87×10^{-6}
0.50	0.0	−0.2	3.71×10^{-3}	−2.4	4.0	0.0	−1.2	2.51×10^{-4}	0.4	0.2	4.80×10^{-3}	−1.0	14.0	−20.0	7.0	1.19×10^{-5}

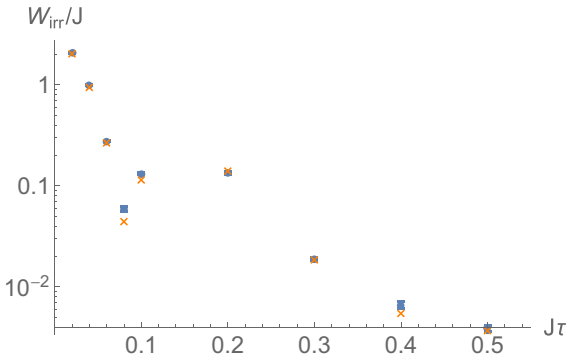

FIG. 7. Plot of the irreversible work vs the duration of the quench τ, evaluated for the exact optimized parameters (orange crosses) and as an average for random fluctuations of these parameters up to the 15% and 5% of the optimal values for A_1 and B_1 respectively (blue dots). These results are obtained for $U_i = 0.2J$ and $U_f = 0.8J$.

We also examine transitions in different regimes, going from an initial value $U_i = 0.8J$ in the Josephson regime to a final one $U_f = 40J$ in the Fock regime. In this case, the most efficient ansatz are $U_{\rm LCS}$ and $U_{\rm 2LCS}$, whose results of the irreversible work are the same from $\tau = 0.02/J$ and for which a zero dissipated work is reached at $\tau = 0.04/J$. It is observed that with the cubic and the quintic the stability is enhanced, although the efficiency is lower, i.e., with the quintic ramp we find a dissipated work equal to zero at $\tau = 0.1/J$ and for the cubic this is obtained at $\tau = 0.4/J$, hence in this case a good compromise between optimization efficiency and stability would be the quintic ramp.

For the two cases examined we have found different results regarding the efficiency and the stability of the optimization, and this can be probably due to the fact that different boundary conditions give different constraints to the values that the parameters can assume. For this reason, we do not expect the kind of parameters landscape such as the one represented in Fig. 5 to be the same in that range of parameter values for transitions with different values of U_i and U_f.

VI. CONCLUSION

In this paper we have analyzed the fluctuations of the work done on an ensemble of ultracold atoms in a two-site Bose-Hubbard model. We have carefully shown analytical predictions for the first two moments of work and the irreversible work for instantaneous quenches. In this regime we have predicted that the probability distribution of work is well described by an exponential function in agreement with that of a quantum harmonic oscillator.

For finite-time ramps, we have analyzed the case of a linear ramp in time demonstrating oscillations of the irreversible work that are synchronous with the squeezing oscillations of the population imbalance distribution. Finally, we have used simple optimal control techniques to minimize the irreversible work to negligible values. This result might have applications in the realization of quantum thermal machines with ultracold atoms and in the quest to maximize their efficiencies.

It is natural to expect further decrease of the irreversible work using a larger chopped basis for the time-dependent ramp. Moreover, one could use more sophisticated schemes as the one in Ref. [28], in which the frequencies of the oscillating terms are chosen random, or the Krotov's method [38]. Our analysis is therefore a starting point for a more systematic study.

Finally, let us discuss possible experimental verifications of our analysis. The two-site Bose-Hubbard model can be realized in different setups with ultracold atoms in double-well potentials, in atomic condensates with two species, and in self-organized condensates in optical cavities [22,25,32,40]. It is worth to stress the fact that (18) is an interesting result because it shows that we can reconstruct the statistics of the work, at least the first two moments, experimentally by measuring only one observable, i.e., the square of the population imbalance, rather than doing two measurements on the energy of the system or by coupling the system to an external quantum probe. Similar experiments could be carried out in nuclear magnetic resonance quadrupolar systems in which spin squeezing has been recently observed [41,42].

ACKNOWLEDGMENTS

The authors thank F. Cataliotti, M. Fattori, I. Mekhov, and J. Sherson for invaluable discussions. This work is supported by the John Templeton Foundation (Grant No. 43467), the EU Collaborative Project TherMiQ (Grant Agreement No. 618074).

APPENDIX: WORK DISTRIBUTION OF A QHO

In this Appendix we revise the dynamics of the parametrically driven quantum harmonic oscillator and how to calculate the work distribution. Let us assume the QHO to be driven with Hamiltonian Eq. (6) from an initial frequency $\omega(0) = \omega_i$ to a final one $\omega(\tau) = \omega_1$. An initial energy eigenfunction of a QHO evolves into [33,43]

$$\psi_n(t) = \frac{1}{2^n n!}\left(\frac{\omega_i}{\pi g_-(t)}\right)^{1/4} H_n\left(\sqrt{\frac{\omega_i}{g_-(t)}}x\right)\cdot \times \exp\left[-\frac{i g_0(t)+\omega_i}{2\pi g_-(t)}x^2 - i\left(n+\frac{1}{2}\right)\int_0^t \frac{\omega_i}{m g_-(t')}dt'\right], \tag{A1}$$

where the H_n are the Hermite polynomials and the functions $g_+(t)$, $g_-(t)$, and $g_0(t)$ satisfy the differential equations

$$\dot{g}_-(t) = -2g_0(t)/m, \tag{A2}$$

$$\dot{g}_0(t) = m\omega^2(t)g_-(t) - g_+(t)/m, \tag{A3}$$

$$\dot{g}_+(t) = 2m\omega^2(t)g_0(t) \tag{A4}$$

with initial conditions $g_-(0) = 1/m$, $g_0(0) = 0$, and $g_+(0) = m\omega_0^2$.

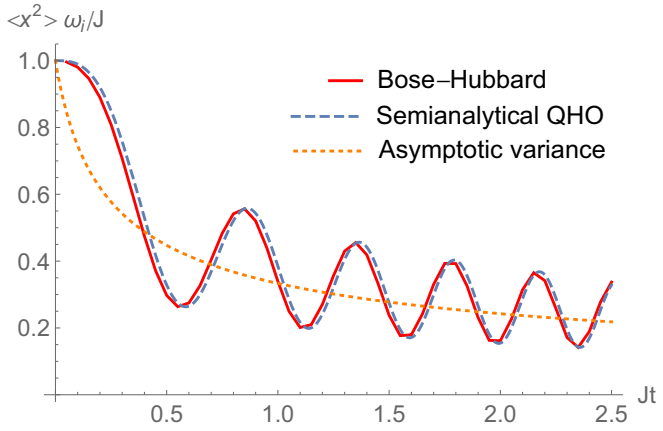

FIG. 8. Comparison of the plots of the variance in units of J/ω_i (where ω_i is the plasma frequency at $t = 0$) vs time obtained for the cases of the numerical Bose-Hubbard model, the semianalytical approach to the QHO and the asymptotic limit. The parameters used are $N = 200$, $U_i = 0$, $U_f = 0.2J$.

Equation (A2) can be used to calculate the position variance of the QHO initially in its ground state $n = 0$:

$$\begin{aligned}\langle x^2\rangle &= \int_{-\infty}^{\infty} |\psi_0(t)|^2 x^2 dx \\ &= \left(\frac{\omega_i}{\pi g_-(t)}\right)^{\frac{1}{2}} \int_{-\infty}^{\infty} dx x^2 \exp\left[2\mathrm{Re}\left(\frac{ig_0(t)-\omega_i}{2g_-(t)}\right)x^2\right] \\ &= \frac{1}{2}\sqrt{\frac{\omega_i}{g_-(t)}}\left[2\mathrm{Re}\left(\frac{ig_0(t)-\omega_i}{2g_-(t)}\right)\right]^{3/2}, \end{aligned} \tag{A5}$$

where in the last passage we used the Gaussian integral $\int e^{-\lambda x^2} x^2 dx = \frac{1}{2}\sqrt{\pi}\lambda^{-3/2}$. It can be noticed that in the case of an adiabatic ramp, since the evolved state at the time τ is an eigenstate of the final Hamiltonian, $\langle x^2\rangle$ will be the variance of the ground state for the final Hamiltonian.

In Fig. 8, we compare the analytical result from (A5) with the one we obtained numerically by using a Trotter expansion of the evolution operator and to the instantaneous variance, defined as $\langle x^2(t)\rangle = J/\omega(t)$. As the frequency $\omega(t)$ is increased, the system wave function tries to catch up with the instantaneous value of the variance and start oscillating around it. The slower the driving, the smaller is the amplitude of these squeezing oscillations.

To calculate the probability distribution of the work we need the transition probability

$$p_{q,0} = |\langle\tilde{\psi}_q|\psi(\tau)\rangle|^2 = \left|\int_{-\infty}^{\infty} dx \tilde{\psi}_q^* \psi_0(\tau)\right|^2, \tag{A6}$$

where we set $n = 0$ as we assume the initial state to be the ground state. To this end, the wave functions of the final Hamiltonian at $t = \tau$, are given by

$$\tilde{\psi}_q = \frac{1}{2^q q!}\left(\frac{m\omega_f}{\pi}\right)^{1/4} \exp\left[\frac{-m\omega_f x^2}{2}\right] H_q(\sqrt{m\omega_f}x). \tag{A7}$$

We thus obtain:

$$p_{q,0} = \left|\int_{-\infty}^{\infty} dx \tilde{\psi}_q \psi_0(\tau)\right|^2 \tag{A8}$$

$$= \left|\frac{1}{2^q q!}\left(\frac{m\omega_f}{\pi}\right)^{1/4}\left(\frac{\omega_i}{\pi g_-(t)}\right)^{1/4} \int_{-\infty}^{\infty} dx H_q(\sqrt{m\omega_f}x) \times \exp\left[\left(\frac{ig_0(t)-\omega_i}{2\pi g_-(t)} - \frac{m\omega_f}{2}\right)x^2\right]\right|^2. \tag{A9}$$

Because of the parity, the only possible transitions that give a nonzero value for the integral above are the ones for which the index q is even, and in this case from (A10) we obtain the result

$$p_{q,0} = \left|\frac{1}{2^q}\left(\frac{m\omega_f\omega_i}{g_-(t)}\right)^{1/4} \frac{1}{(q/2)!} \times \frac{[(ig_0(t)-\omega_i)/(2\pi g_-(t)) - m\omega_f/2 + \sqrt{m\omega_f}]^{q/2}}{[-(ig_0(t)-\omega_i)/(2\pi g_-(t)) + m\omega_f/2]^{(q+1)/2}}\right|^2, \tag{A10}$$

where we used the result

$$\int \exp[\alpha x^2] H_q(\beta x) dx = \frac{q!\sqrt{\pi}}{(q/2)!}\frac{(\alpha+\beta)^{q/2}}{(-\alpha)^{(q+1)/2}}.$$

[1] C. Jarzynski, Phys. Rev. Lett. **78**, 2690 (1997).
[2] G. E. Crooks, Phys. Rev. E **60**, 2721 (1999).
[3] P. Talkner, E. Lutz, and P. Hänggi, Phys. Rev. E **75**, 050102 (2007).
[4] M. Campisi, P. Hänggi, and P. Talkner, Rev. Mod. Phys. **83**, 771 (2011).
[5] G. Watanabe, B. P. Venkatesh, P. Talkner, M. Campisi, and P. Hänggi, Phys. Rev. E **89**, 032114 (2014).
[6] A. J. Roncaglia, F. Cerisola, and J. P. Paz, Phys. Rev. Lett. **113**, 250601 (2014).
[7] G. De Chiara, A. J. Roncaglia, and J. P. Paz, New J. Phys. **17**, 035004 (2015).
[8] P. Talkner and P. Hanggi, Phys. Rev. E **93**, 022131 (2016).
[9] L. Fusco, S. Pigeon, T. J. G. Apollaro, A. Xuereb, L. Mazzola, M. Campisi, A. Ferraro, M. Paternostro, and G. De Chiara, Phys. Rev. X **4**, 031029 (2014).
[10] I. Bloch, J. Dalibard, and W. Zwerger, Rev. Mod. Phys. **80**, 885 (2008).
[11] I. M. Georgescu, S. Ashhab, and F. Nori, Rev. Mod. Phys. **86**, 153 (2014).
[12] M. Lewenstein, A. Sanpera, and V. Ahufinger, *Ultracold Atoms in Optical Lattices* (Oxford University Press, Oxford, 2012).
[13] J. Eisert, M. Friesdorf, and C. Gogolin, Nature Phys. **11**, 124 (2015).
[14] A. Polkovnikov, K. Sengupta, A. Silva, and M. Vengalattore, Rev. Mod. Phys. **83**, 863 (2011).
[15] B. D. Josephson, Phys. Lett. **1**, 251 (1962).
[16] J. Javanainen, Phys. Rev. Lett. **57**, 3164 (1986).
[17] A. Smerzi, S. Fantoni, S. Giovanazzi, and S. R. Shenoy, Phys. Rev. Lett. **79**, 4950 (1997).
[18] G. J. Milburn, J. Corney, E. M. Wright, and D. F. Walls, Phys. Rev. A **55**, 4318 (1997).

[19] A. J. Leggett, Rev. Mod. Phys. **73**, 307 (2001).
[20] B. Juliá-Díaz, D. Dagnino, M. Lewenstein, J. Martorell, and A. Polls, Phys. Rev. A **81**, 023615 (2010).
[21] S. Barzanjeh and D. Vitali, Phys Rev. A **93**, 033846 (2016).
[22] M. Albiez, R. Gati, J. Fölling, S. Hunsmann, M. Cristiani, and M. K. Oberthaler, Phys. Rev. Lett. **95**, 010402 (2005).
[23] R. Gati and M. K. Oberthaler, J. Phys. B **40**, R61 (2007).
[24] Y. Shin, M. Saba, T. A. Pasquini, W. Ketterle, D. E. Pritchard, and A. E. Leanhardt, Phys. Rev. Lett. **92**, 050405 (2004).
[25] T. Schumm, S. Hofferberth, L. M. Andersson, S. Wildermuth, S. Groth, I. Bar-Joseph, J. Schmiedmayer, and P. Krüger, Nature Phys. **1**, 57 (2005).
[26] T. Zibold, E. Nicklas, C. Gross, and M. K. Oberthaler, Phys. Rev. Lett. **105**, 204101 (2010).
[27] K. Maussang, G. E. Marti, T. Schneider, P. Treutlein, Y. Li, A. Sinatra, R. Long, J. Estève, and J. Reichel, Phys. Rev. Lett. **105**, 080403 (2010).
[28] P. Doria, T. Calarco, and S. Montangero, Phys. Rev. Lett. **106**, 190501 (2011).
[29] A. E. Allahverdyan and T. M. Nieuwenhuizen, Phys. Rev. E **71**, 046107 (2005).
[30] H. J. Lipkin, N. Meshkov, and A. Glick, Nucl. Phys. **62**, 188 (1965).
[31] P. Ribeiro, J. Vidal, and R. Mosseri, Phys. Rev. E **78**, 021106 (2008).
[32] F. Brennecke, R. Mottl, K. Baumann, R. Landig, T. Donner, and T. Esslinger, Proc. Natl. Acad. Sci. **110**, 11763 (2013).
[33] I. J. Ford, D. S. Minor, and S. J. Binnie, Eur. J. Phys. **33**, 1789 (2012).
[34] S. Deffner and E. Lutz, Phys. Rev. E **77**, 021128 (2008).
[35] P. Salamon, K. H. Hoffmann, Y. Rezek, and R. Kosloff, Phys. Chem. Chem. Phys. **11**, 1027 (2009).
[36] F. Galve and E. Lutz, Phys. Rev. A **79**, 032327 (2009).
[37] M. V. S. Bonança and S. Deffner, J. Chem. Phys. **140**, 244119 (2014).
[38] V. Krotov, *Global Methods in Optimal Control Theory*, Vol. 195 (CRC Press, Boca Raton, 1995).
[39] K. W. Moore and H. Rabitz, Phys. Rev. A **84**, 012109 (2011).
[40] S. van Frank, A. Negretti, T. Berrada, R. Bücker, S. Montangero, J. F. Schaff, T. Schumm, T. Calarco, and J. Schmiedmayer, Nature Commun. **5**, 4009 (2014).
[41] R. Auccaise, A. G. Araujo-Ferreira, R. S. Sarthour, I. S. Oliveira, T. J. Bonagamba, and I. Roditi, Phys. Rev. Lett. **114**, 043604 (2015).
[42] A. G. Araujo-Ferreira, R. Auccaise, R. S. Sarthour, I. S. Oliveira, T. J. Bonagamba, and I. Roditi, Phys. Rev. A **87**, 053605 (2013).
[43] K. Husimi, Prog. Theor. Phys. **9**, 381 (1953).